

Substrate-dependent pore formation in molybdenum disulfide monolayers under ion irradiation

Yossarian Liebsch,^{*,†} Umair Javed,[‡] Lucia Skopinski,[†] Leon Daniel,[†] Franziska Appel,[†] Radia Rahali,[¶] Clara Grygiel,[¶] Henning Lebius,[¶] Carolin Frank,[†] Lars Breuer,[†] Leon Kirsch,[§] Frieder Koch,[§] Jani Kotakoski,[‡] and Marika Schleberger[†]

[†]*Fakultät für Physik and CENIDE, Universität Duisburg-Essen, 47057 Duisburg, Germany*

[‡]*Faculty of Physics, University Vienna, -1090 Vienna, Austria*

[¶]*CIMAP-GANIL, CEA-CNRS-ENSICAEN-UCN, Caen, 14076, France*

[§]*GSI Helmholtzzentrum für Schwerionenforschung, Planckstr. 1, 64291, Darmstadt, Germany*

E-mail: yossarian.liebsch@uni-due.de

Phone: +49 (203) 379 2321

Abstract

Ion irradiation is a versatile tool for nanostructuring surfaces, yet the roles of energy deposition and dissipation at the surface and in ultrathin materials remain poorly understood. In this study, we investigate nanopore formation in monolayer MoS₂ on different substrates under irradiation of highly charged ions (HCIs) and swift heavy ions (SHIs): two types of ions that, despite having vastly different kinetic energies, interact primarily with the electronic system of the target. Using scanning transmission electron microscopy, we quantify pore radii and pore formation efficiencies for suspended MoS₂,

MoS₂ on SiO₂, bilayer MoS₂ and MoS₂ on gold. Both pore size and pore formation efficiency exhibit a pronounced dependence on the type of substrate. Pores are largest and most frequent in MoS₂ on SiO₂, while the gold substrate massively quenches pore formation. The results indicate that the observed pore dimensions under both HCI and SHI irradiation are consistent with a central role of substrate and interface-dependent electronic dissipation pathways.

Introduction

Ion beams provide a controllable route to engineer defects in two-dimensional materials, enabling property tuning from doping to nanopore formation.¹⁻⁴ Because kinetic energy, charge state, and mass can be varied over wide ranges, ion irradiation offers a large parameter space for nanostructuring. Achieving predictive control requires a detailed understanding of ion–solid interaction and post-impact energy dissipation.⁵ While bulk ion–solid interactions are well described across many energy regimes,⁶⁻⁸ the interaction with surfaces and ultrathin targets—particularly for highly charged ions (HCIs) and swift heavy ions (SHIs)—remains less complete.

The emergence of two-dimensional (2D) materials has intensified interest in ion–surface interactions.⁹⁻¹³ Owing to their atomic thickness, 2D materials combine outstanding mechanical properties with promising (opto-)electronic and catalytic functionality.¹⁴⁻¹⁸ Ion irradiation has proven effective for defect engineering across regimes: low-energy ions enable implantation with near-atomic precision,¹⁹⁻²¹ keV ions primarily create point defects in monolayers,^{22,23} and HCIs add potential energy that can drive larger defect complexes.²⁴ At MeV energies, damage is dominated by electronic excitation and can be tuned by the irradiation geometry (e.g., grazing incidence).^{25,26}

While fundamental studies of ion irradiation-induced defect formation have largely focused on suspended 2D materials,^{13,24,27,28} practical applications typically require the 2D material to be supported by a substrate. Direct investigation of ion-irradiated supported 2D

materials, however, remains experimentally challenging for several reasons. High-resolution STEM generally requires freestanding membranes, while atomic-resolution AFM and STM demand exceptionally clean surfaces and can further complicate interpretation, since both topographic and electronic contrast may contain contributions from the substrate as well as from the 2D layer.^{29–32} As a result, many studies of supported systems rely on Raman, photoluminescence, or electrical measurements, which are sensitive to electronic and strain-related changes but do not directly resolve the atomic structure.^{33,34}

This leaves a gap in our understanding of how ion-induced defect formation differs between suspended and substrate-supported 2D materials. We address this gap by directly measuring substrate effects on defect formation in MoS₂ under HCI and SHI irradiation. HCIs and SHIs represent two distinct irradiation regimes with vastly different kinetic energies and energy-deposition profiles. HCIs release their potential energy predominantly through ultrafast charge exchange and Auger-type processes near the surface,^{35,36} whereas SHIs deposit energy continuously along their trajectory via electronic stopping S_e . Despite these differences, both ion types couple primarily to the electronic system of the target, such that subsequent energy transfer to the lattice is governed by electron–phonon coupling.^{37,38} This makes HCI and SHI irradiation a useful pair of probes for testing how substrate-controlled electronic dissipation influences defect formation in 2D materials.

Here we directly quantify how substrate coupling influences electronically driven defect formation in monolayer MoS₂. Using scanning transmission electron microscopy, we measure pore radii and pore formation efficiencies after irradiation in several configurations (suspended, supported on SiO₂, bilayer, and metal-supported samples). We compare HCIs and SHIs as complementary excitation regimes with distinct energy-deposition profiles but a shared dependence on post-impact electronic energy dissipation. Owing to this common feature, we expect the substrate may influence pore formation in a qualitatively similar way for both ion types.

Results and discussion

Highly Charged Ions

In order to assess substrate effects under HCI irradiation, we compare monolayer MoS₂ on SiO₂/Si with suspended MoS₂ reported by Kozubek et al.²⁴ Using the same ion species and kinetic energies as in that work, we vary the charge state to deliver between 15 – 40 keV of potential energy to the surface. In contrast to earlier AFM studies on supported samples that suggested pronounced topographic changes but could not resolve the defect structure,^{39,40} our STEM analysis shows that irradiation on SiO₂ produces well-defined, pore-shaped defects with no obvious long-range lattice distortion of the surrounding material (see Fig.S1), consistent with the pore morphology previously reported for suspended MoS₂.²⁴ Representative pores are shown in Fig. 1a-d.

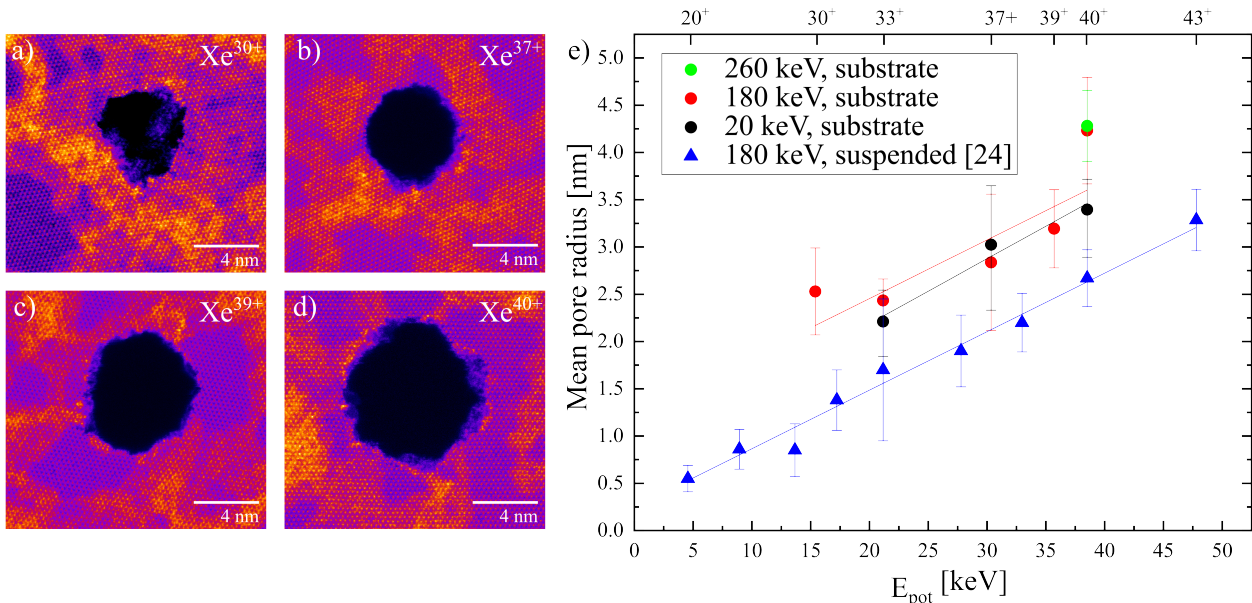


Figure 1: (a-d) False-color STEM images of pores in single-layer MoS₂ created by Xe ions with different charge states at 180 keV. Orange structures are caused by hydrocarbon contamination. (e) Mean pore radii of SL-MoS₂ on SiO₂/Si substrate irradiated with highly charged Xe ions at different kinetic energies (green, red, black). Pore radii are larger when MoS₂ is irradiated on SiO₂ compared to the suspended configuration (blue, data by Kozubek *et al.*)²⁴

We quantified pore-size distributions by measuring (~ 150) pores. Mean pore radii are

summarized in Fig. 1e. For both supported and suspended samples, the mean radius increases approximately linearly with the projectile potential energy. Within uncertainty, the slopes are similar for supported and suspended (0.06–0.07 nm/keV), indicating comparable scaling with charge state. Pores on SiO₂ are systematically larger by ~ 1 nm across all charge states. In addition, within our experimental resolution we observe no significant dependence of pore radius on kinetic energy over the investigated range.

This observation is consistent with sputtering experiments of SL-MoS₂ carried out by Skopinski *et al.*, who found that the sputtering yield of Mo is significantly more sensitive to changes in the charge state of the HCI rather than its kinetic energy.⁴¹ These observations suggest that nuclear sputtering contributes only weakly under the present conditions and pore formation is dominated by the deposition and dissipation of the HCI’s potential energy.

Charge-exchange studies for HCIs on 2D materials carried out by Creutzburg *et al.* and Niggas *et al.* found that the majority of the HCIs potential energy ($\sim 80 - 90\%$) is deposited *via* Auger processes in the electronic system of the first layer of the target 2D material, independent of the materials electronic properties.^{28,42} Linking the charge exchange to pore formation, Grosseck *et al.* introduced a model for nanopore formation in graphene, that centers around the target’s charge carrier mobility.⁴³ They argue that the high electron mobility of graphene leads to a fast charge dissipation in the 2D material, effectively suppressing pore formation. As a consequence, HCI irradiation does not create pores in graphene (typically $\geq \mu = 60.000 \text{ cm}^2 \text{ V}^{-1}\text{s}^{-1}$ for suspended graphene⁴⁴), but very likely in MoS₂, which has a significantly smaller electron mobility (typically $\mu \approx 1 - 10 \text{ cm}^2 \text{ V}^{-1}\text{s}^{-1}$ for suspended MoS₂^{45,46}).

Building on the model introduced by Grosseck *et al.*, in which charge carrier mobility governs the efficiency of pore formation under HCI irradiation,⁴³ the larger pores observed in MoS₂ on SiO₂ can be interpreted in terms of substrate-modified electronic energy dissipation within the MoS₂ layer. For an insulating substrate, out-of-plane dissipation remains limited. However, substrate-induced disorder and charge trapping are expected to increase carrier

scattering, thereby limiting lateral spreading of the non-equilibrium electronic excitation. This is known from several studies on charge transport in MoS₂ that report higher carrier mobility in suspended monolayers than in MoS₂ on SiO₂.^{47,48} Reduced mobility can slow lateral charge redistribution, which may increase the spatial localization of the transient excitation and thus raise the local electronic energy density. This in turn may increase the local energy density available for lattice excitation. We note that this interpretation is inferential—the dissipation pathway is not measured directly—but it is consistent with the pore size enhancement observed under both HCI and SHI irradiation (see Fig. 4 a), suggesting the effect is not specific to one excitation regime.

The preceding discussion focused on lateral (in-plane) dissipation pathways, treating out-of-plane dissipation as negligible for an insulating substrate. If, however, a semiconducting or metallic substrate is used, this additional dissipation channel could strongly influence pore formation. Multilayer MoS₂ provides a controlled way to introduce out-of-plane dissipation without changing the substrate material. Although adjacent layers are coupled only weakly via van-der-Waals forces, a second (or third) MoS₂ layer can act as an additional reservoir for charge and excitation redistribution relative to an isolated monolayer, offering a simplified analogue of out-of-plane dissipation into a semiconducting environment.

To test the role of out-of-plane electronic energy dissipation, we exploit regions of different thickness in CVD-grown MoS₂ (Fig. 2a). Compared to monolayer regions (1L), bilayer MoS₂ (2L) shows both reduced pore radii and reduced pore formation efficiency (Fig. 2b). In trilayer regions (3L), fully penetrating pores are strongly suppressed and partially penetrating (non-through) pores occur (Fig. 2c). These observations indicate that out-of-plane electronic energy dissipation is present but limited in magnitude: coupling to a second layer is sufficient to modify pore formation, yet the available excitation appears insufficient to efficiently drive a fully penetrating defect through three layers.

The observed anisotropy of the defects (radius \approx 2.2 nm; depth \approx 1.5 nm) likely reflects the strongly different in-plane and out-of-plane dissipation pathways in layered MoS₂,^{49,50}

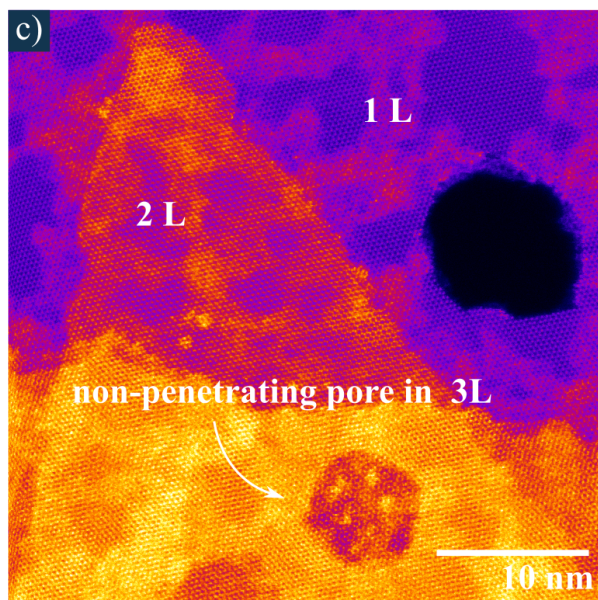
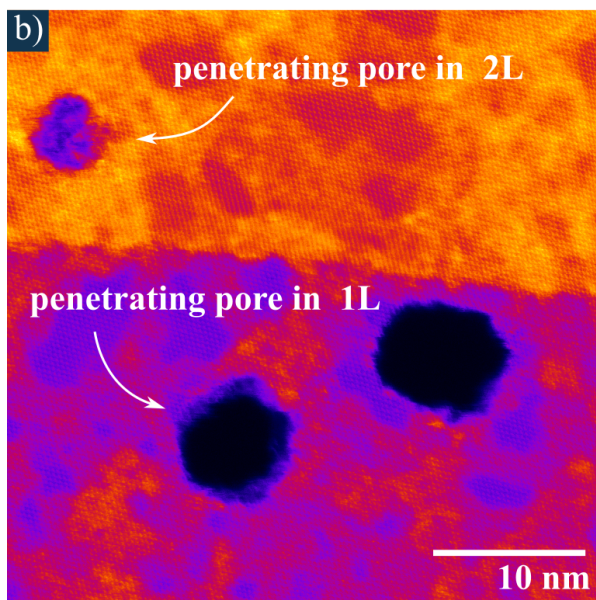
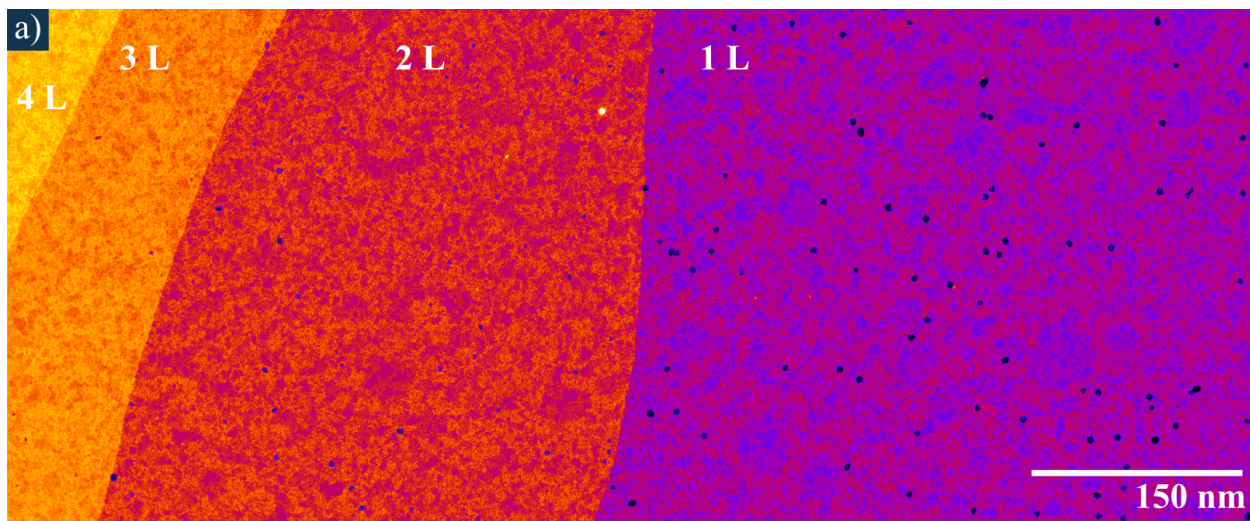


Figure 2: (a) STEM images of MoS₂ on SiO₂ with different layer numbers, irradiated with 180 keV Xe³⁷⁺ ions. (b) Fewer and smaller pores are observed in bilayer MoS₂ (2L) compared to monolayer on SiO₂ (1L). (c) In trilayer MoS₂, pores are predominately non-penetrating.

which disfavor spherical damage volumes.

Swift Heavy Ions

In addition to HCI irradiation, we investigate samples irradiated with SHIs. SHIs deposit energy continuously along their trajectory via electronic stopping S_e , producing excitation and ionization of the target’s electronic system (Fig. 3).^{51,52} This extended deposition profile provides a complementary probe of substrate-controlled electronic energy dissipation. Based on previous results on suspended MoS₂, the SHIs used in this study are expected to deposit in the order of ~ 10 keV (0.7 MeV/u Xe²³⁺) and ~ 20 keV (4.8 MeV/u Au²⁵⁺) in a monolayer.¹³

In Fig. 3, representative multilayer regions after HCI and SHI irradiation are shown. Pores in monolayers are of comparable size, while the penetration behavior differs strongly. Quantitative pore radii and pore formation efficiencies for all configurations are summarized in Fig. 4. For both ion types, monolayer MoS₂ on SiO₂ exhibits the largest pores. However, thickness affects the two regimes differently: under SHI irradiation pore size and efficiency depend only weakly on layer number, whereas HCI-induced pore formation attenuates rapidly with thickness. This contrast is consistent with SHIs transferring electronic energy along an extended track deep into the target, while HCIs release their potential energy predominantly near the surface during a single neutralization event.

The pronounced difference in size and efficiency between suspended and supported MoS₂ under SHI irradiation is consistent with the strong impact-parameter dependence of electronic energy deposition in an atomically thin target.¹³ In suspended monolayers, a significant fraction of ion passages yields local energy densities that remain below the threshold for pore formation, depending on the trajectory relative to atomic sites. Adding a substrate and/or additional layers reduces the likelihood of such “sub-threshold” events because energy deposition and subsequent dissipation are distributed across coupled layers. Moreover, we previously showed that pore formation under SHI irradiation is strongly quenched by energy loss through particles escaping from both sides of a suspended membrane.¹³ A substrate

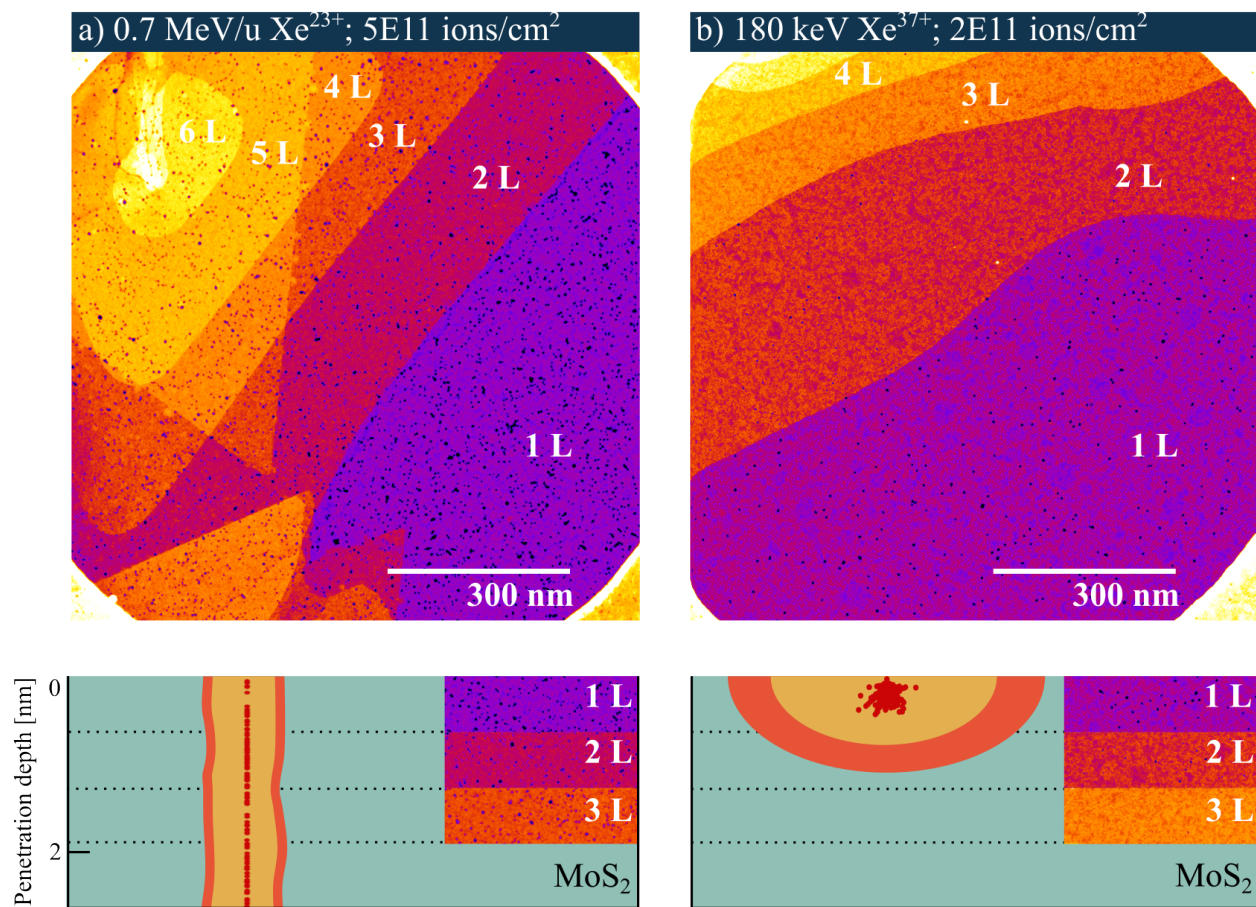


Figure 3: Comparison of SHI-irradiated (a) and HCI-irradiated (b) MoS₂ reveals similar pore dimensions in 1L, but, as expected, vastly different penetration behavior. Schematics below each image illustrate energy deposition profiles of the different irradiation types. Note that these illustrations are visual representations and not to scale.

hinders this loss channel by restricting escape to one side, further increasing the effective energy available for damage formation.

For HCIs, the initial interaction is governed by near-surface charge exchange within a nm-scale zone spanning multiple atoms.^{53,54} This may reduce sensitivity to atomic-scale impact parameter compared to the SHI impact.

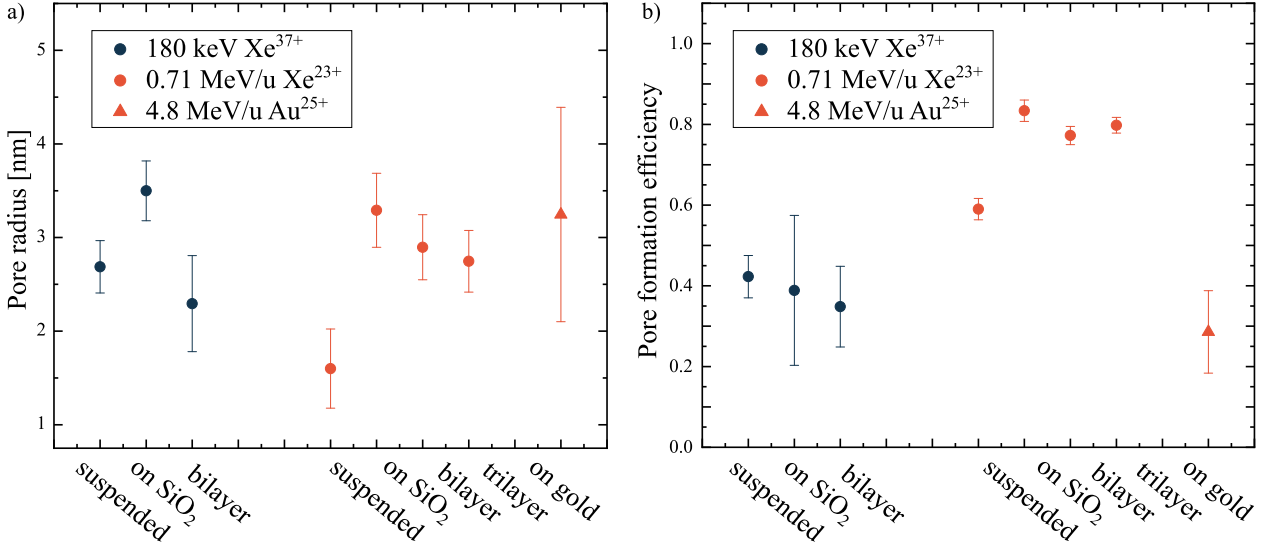


Figure 4: Mean pore radii (a) and pore formation efficiencies (b) of HCI and SHI-irradiated MoS₂ in different configurations. Error bars of mean pore radii are the standard deviation, while uncertainty in efficiency arises from pore counting and fluence determination in all cases, and for HCI-irradiated supported samples additionally from partial-area irradiation, transfer-related misalignment (see Fig.S3).

We observe that the pore formation efficiencies differ for the two ion types. Pore formation efficiency is here defined as the number of pores per incident ion. It is measured using large STEM images containing ~ 100 pores (see Supporting Information). HCIs yield generally lower efficiencies ($\eta \sim 0.4$) for the same target configuration than SHIs ($\eta \sim 0.6 - 0.9$). HCI efficiencies carry larger systematic uncertainty, arising from a fluence gradient across the beam spot and the transfer-related misalignment (Fig. S3), and should therefore be interpreted with caution. An additional source of local suppression is hydrocarbon contamination: ambient exposure produces hydrocarbon coverage on 2D materials,⁵⁵ and we observe indications of locally reduced pore formation in contaminated regions (Fig. S5), which likely

lowers the apparent efficiency in the case of HCl.

For SHI irradiation, efficiency data are more meaningful. Efficiency in supported MoS₂ approaches saturation ($\eta \sim 0.8$), whereas efficiency in the suspended monolayer remains well below saturation $\eta \approx 0.6$. This behavior can, again, be traced back to sub-threshold energy transfer impacts that can occur in monolayers.¹³ The notably low efficiency observed for MoS₂ on Au ($\eta \approx 0.28$) stands apart from this trend and will be discussed further below.

A remaining question is whether pore formation can be mitigated by the right choice of substrate. Schweska *et al.* demonstrated that graphene/MoS₂ heterostructures can be resistant to HCl-induced pore formation when MoS₂ is covered by graphene, as charge exchange and potential energy deposition primarily occurs within the graphene.²⁷ Importantly, when the heterostructure is inverted such that the HCl reaches MoS₂ first, pores are still created in MoS₂.

This behavior is consistent with the weak coupling of different layers in van-der-Waals heterostructures. Although graphene is an excellent in-plane conductor, the out-of-plane electrical (and thermal) coupling across the graphene/MoS₂ interface is comparatively weak.^{56,57} Simulations by Schweska *et al.* suggest that the out-of-plane conductance across the graphene/MoS₂ interface is two orders of magnitude smaller than the in-plane conductance of the individual layers.²⁷ Consistent with limited charge transfer between MoS₂ and graphene, no strong PL quenching through loss of photoexcited charge carriers from the MoS₂ into the graphene is observed in graphene/MoS₂ heterostructures.⁵⁸

In contrast, coupling between 2D semiconductors and Au can be substantially stronger, which underlies the success of Au-assisted exfoliation and the formation of large-area, clean interfaces.^{59,60} Motivated by this, we irradiated MoS₂ exfoliated on Au to test whether a metallic substrate with strong interfacial coupling can act as an efficient sink for transient electronic excitation and charge, thereby suppressing pore formation under electronically dominated ion impact.

In contrast to the samples discussed above, for which MoS₂ was transferred after irradi-

ation using only water, transfer from Au substrates to TEM grids requires chemical removal of the gold support using an iodine/iodide etchant (KI/I₂). Consequently, unlike in the previous case, the ion-induced pores cannot be assumed to remain unaffected during transfer,⁶¹ as they were in the previous case. For this reason, the pore formation efficiency is expected to be the more reliable observable for a quantitative discussion of this substrate, whereas pore dimensions can only be discussed qualitatively.

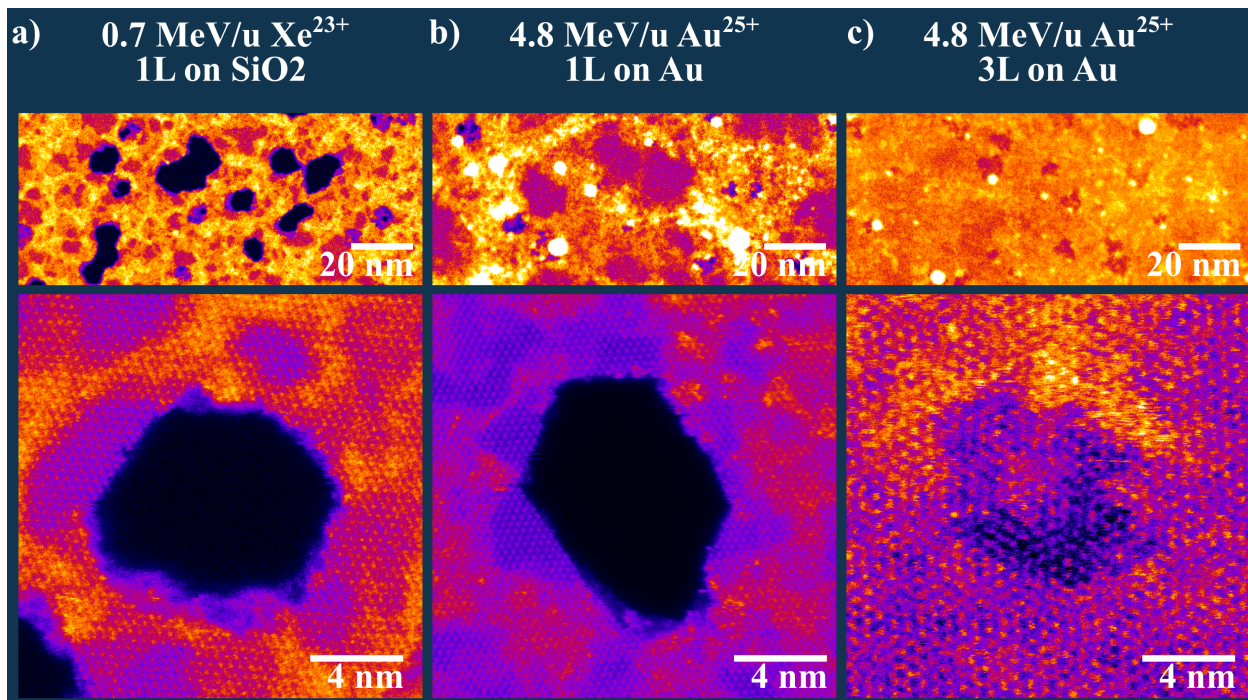


Figure 5: Comparison of SL-MoS₂ irradiated on SiO₂ (a) and on gold substrate (b). On gold, pore formation efficiency is strongly reduced compared to MoS₂ on SiO₂. In addition, the expected increase in pore dimensions due to the difference in predicted stopping power between the two irradiations is not observed. (c) In trilayer MoS₂ on Au, only a single layer is penetrated, as evidenced by the Moiré pattern (caused by bilayer MoS₂) present on top of the pore. Bright, white spots in the STEM images are caused by dense agglomerates that can either stem from irradiation (Mo) or the transfer (Au). The lighter orange color of the trilayer image compared to monolayer originates from thickness-dependent scattering of electrons.

Fig. 5 compares SHI-irradiated MoS₂ on SiO₂ (a) with MoS₂ irradiated on Au (b). The two irradiations use different ions: the electronic stopping power of 4.8 MeV/u Au²⁵⁺ in suspended MoS₂ is approximately double that of 0.71 MeV/u²³⁺ Xe,¹³ such that larger

pores would be expected on Au in the absence of substrate effects, as previously shown for suspended MoS₂.¹³ Instead, pores of similar dimension to those on SiO₂ are observed (Fig. 4 a). The pores on Au additionally exhibit a broad size distribution and an unusual morphology (see Fig.S6 and Fig.S7), with many showing straight, lattice-aligned edges consistent with faceted etch pits.⁶² We interpret this as evidence of the aforementioned influence of the etchant during transfer, which may bias the measured pore sizes toward larger values.⁶³

All irradiations shown in Fig. 5 were performed at the same fluence ($5 \times 10^{11} \text{ cm}^{-2}$). The pore formation efficiency of MoS₂ on Au is strongly reduced ($\eta \approx 0.28$) compared with MoS₂ on SiO₂ ($\eta \approx 0.83$). In trilayer regions of the same sample (Fig. 5 c), a new type of defect is observed: here, only one of the three layers is perforated. This is apparent from the Moirè pattern observed on top of defects (c) that only appears if at least two layers of MoS₂ are present. These non-penetrating defects in trilayer MoS₂ occur at a much higher rate ($\eta \approx 0.89$) than penetrating-pores in the monolayer regions. We interpret this contrast as evidence that the Au substrate acts as an efficient sink for electronic excitation generated in the first two MoS₂ layers near the interface, reducing the electronic energy density retained in MoS₂ below the threshold for pore formation. The high efficiency in the trilayer case is consistent with this picture: in the outermost layer, sufficiently far from the Au interface, dissipation into the substrate is reduced and the local excitation can exceed the formation threshold. As discussed for SHI-irradiated suspended MoS₂,¹³ pore formation efficiency is highly sensitive to threshold shifts, explaining why the efficiency changes drastically between 1L and 3L while pore sizes remain comparable.

The inferred efficient out-of-plane dissipation from MoS₂ into Au is consistent with the well-known strong MoS₂-Au interfacial coupling. Our own Raman and PL characterization of the MoS₂/Au samples (see Fig.S2) shows splitting of the out-of-plane A_{1g} mode and strong PL quenching relative to MoS₂ on SiO₂, indicating that the interface modifies both lattice dynamics and carrier recombination in the as-prepared samples. The microscopic origin of this coupling has been attributed to Fermi-level pinning arising from interface-

dipole formation and the appearance of Mo d-orbital gap states due to metal–S interactions at the interface.^{60,64} Whether these equilibrium coupling mechanisms directly govern the efficiency of transient charge transfer under ion impact remains an open question, but the consistency between the strong equilibrium coupling and the observed suppression of pore formation supports the interpretation that Au provides an efficient dissipation channel for electronically driven damage.

The trends in pore size and pore formation efficiency observed here are robust, but the underlying dissipation pathways are inferred indirectly from defect statistics rather than measured directly. These limitations do not alter the main comparative conclusions, but they constrain the level of mechanistic interpretation that can be drawn from the present dataset.

Conclusion

We have shown that substrate coupling plays a decisive role in electronically driven pore formation in MoS₂ under both HCI and SHI irradiation. An insulating substrate increases pore size in comparison to suspended membranes, out-of-plane energy dissipation redistributes energy and suppresses pore formation in MoS₂ multilayers, and a strongly coupled metallic substrate (Au) markedly reduces the pore formation efficiency. Together, these trends indicate that, for ions that primarily interact with the electronic system of the target, pore evolution is governed less by the energy deposition mechanism than by how efficiently that electronic excitation is redistributed and converted into lattice motion under the constraints imposed by the interface. The presented substrate- and thickness-resolved pore statistics provide quantitative benchmarks for future modeling. The most promising next step is likely not a full atomistic treatment of the entire ion impact, but instead a targeted description of electronic energy dissipation across the interface between the 2D material and the substrate.

Methods and Materials

Sample Preparation

A custom chemical vapor deposition (CVD) process is used to grow monolayer MoS₂. Substrates are prepared by placing a micro droplet of saturated ammonium heptamolybdate (AHM) onto 300 nm SiO₂/Si substrate. The substrates are then spin-coated with a 1% sodium cholate solution that acts as a growth promoter. Substrates are then placed into the second zone of a three-zone furnace. In the first zone ~ 60 mg of sulfur is placed. An Argon flow of 500 sccm is used to purge the quartz tube containing the reagents and as means to transport the precursors. During the 30 min long process, the first zone reaches 150 °C, while the second zone reaches 750 °C. After the process has finished, the furnace is opened to allow for rapid cooling. The freshly grown MoS₂ flakes are irradiated on the SiO₂/Si substrate and subsequently transferred to a QUANTIFOIL© holey carbon grid with 1.2 μ m holes. The transfer is performed by placing the TEM-grid onto the sample with the mesh facing the MoS₂ side. By placing a droplet of water near the grid, the water can intercalate between the flakes and the substrate, lifting off the MoS₂ in the process and pressing it against the QUANTIFOIL© holey carbon mesh. Sample preparation and characterization are schematically shown in Fig. 6.

To investigate the irradiation of MoS₂ on Au, a substrate suitable for mechanical exfoliation is first prepared. A 5 nm Ti adhesion layer is deposited onto SiO₂, followed by the deposition of a 25 nm Au film. Immediately after deposition, MoS₂ is mechanically exfoliated onto the freshly prepared Au surface.

After irradiation on Au, the monolayers had to be transferred onto TEM grids for STEM characterization. For this purpose, a thin polystyrene (PS) layer is spin-coated onto the sample. The sample is then immersed in a preheated KI/I₂ etching solution (4 g KI, 1.1 g I, 150 ml H₂O) at 40 °C. After approximately 1 h, the Au layer has dissolved, allowing the PS film with the attached monolayers to be retrieved and cleaned in ultrapure water.

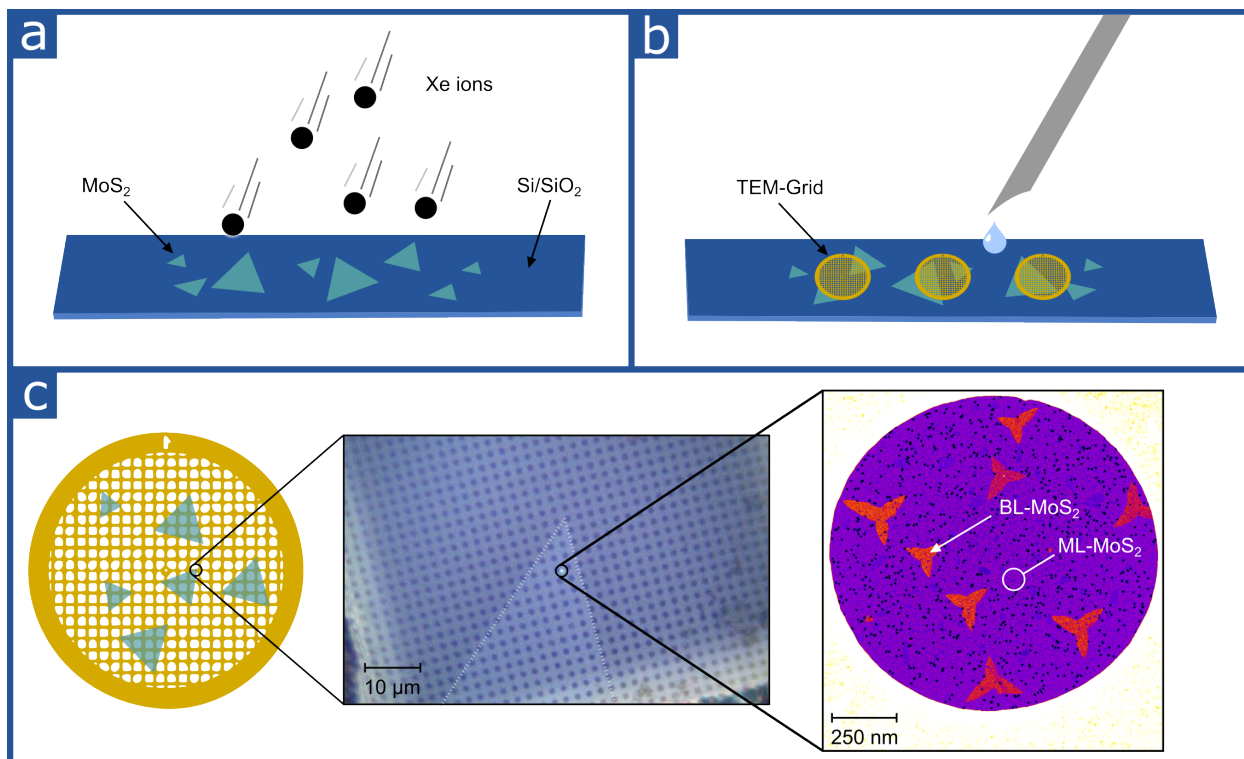


Figure 6: Schematic of the irradiation and subsequent STEM analysis of MoS₂ on SiO₂. First, CVD-grown MoS₂ on SiO₂/Si is irradiated with highly charged ions (a). After that irradiated MoS₂ is transferred polymer-free to a TEM-Grid (b). (c) Transferred flakes on the TEM-grid (left) are visible in an optical microscope (center). On the right, a STEM image of a single TEM-Grid pore, covered by monolayer (ML) and occasionally bilayer (BL) MoS₂ is shown.

The film is then transferred onto a TEM grid and heated for 30 min at 80 °C, followed by 1 h at 130 °C. During this step, slow heating and cooling are essential to avoid damaging the TEM grid. Finally, the PS film is dissolved in toluene for 2 h, with the solvent renewed once during the process. After retrieval, the grid is immersed in analytical-grade isopropanol as a final cleaning step and then left to dry.

Ion irradiation

Irradiation with highly charged Xenon ions was done at the HICS beamline at the University of Duisburg-Essen.^{41,65,66} The ions with charge states $q=28+$ up to $q=44+$ are provided by an electron beam ion source (EBIS). Samples were irradiated under perpendicular incidence with a fluence of $\Phi=5\times 10^{11}\text{ cm}^{-2}$. At this fluence the density of pores is high enough to image them efficiently in the STEM, while it is low enough to avoid frequent occurrence of overlapping pores (see Supplementary Information). Irradiation was performed at three different kinetic energies (20 keV, 180 keV, 260 keV) in order to evaluate the influence of the kinetic energy on the pore creation. As there was no evidence for differences between the two high energies, no additional irradiations at 260 keV after the initial one were done. Irradiation with SHIs was performed at IRRSUD at GANIL, Caen (0.7 MeV/u $^{129}\text{Xe}^{23+}$) and at M-Branch at GSI, Darmstadt (4.8 MeV/u $^{197}\text{Au}^{25+}$). For both irradiations flux was kept below $1\times 10^9\text{ s}^{-1}\text{ cm}^{-2}$ to avoid thermal damage. Total fluence was again set to $\Phi=5\times 10^{11}\text{ cm}^{-2}$. All irradiations were under perpendicular incidence.

Imaging

Scanning transmission electron microscopy (STEM) measurements were carried out in Vienna with an aberration corrected Nion UltraSTEM 100. Prior to imaging, the samples were heated at 170°C for around 10 h in vacuum to minimize the amount of surface contamination, and inserted into the microscope without air exposure.⁶⁷ The images were recorded with medium angle annular dark field (MAADF) detector with a collection semiangle of

60-200 mrad. Acceleration voltage of electrons was 60 kV and a dwell time of 8 $\mu\text{s}/\text{px}$ and a flyback time of 120 μs were used to record images with 1024×1024 px. Images were recorded at fields of view of 32 nm for the pore sizes analysis and 512 nm for obtaining an overview. At least 150 pores were analyzed for each set of ion irradiation parameters. As most of the pores display round shapes, the area was converted to pore radii r according to $A = \pi r^2$.

Raman and PL spectroscopy

Raman and PL spectroscopy were performed using a WITec alpha300 RA confocal Raman spectrometer. In all instances a green laser ($\lambda = 532$ nm) with a maximum power of 1 mW was used. For Raman spectra a 1800 lmm^{-1} grating was used, while a 300 lmm^{-1} grating was used for PL recording.

Acknowledgement

UJ and JK acknowledge funding from the Austrian Science Fund (FWF) within the Cluster of Excellence MECS (DOI: 10.55776/COE5). Y.L, M.S, L.S, L.D, C.F and L.B thank the Deutsche Forschungsgemeinschaft (DFG, German Research Foundation) for the support of this work under project numbers 272132938, 429784087 and 501495566, and through IRTG 2803 “2D Mature” (project number 461605777; P05), as well as project numbers 501495566 and 272132938. Results presented here are partly based on experiments performed at the beam line M3 at the GSI HelmholtzZentrum für Schwerionenforschung, Darmstadt (Germany) in the context of FAIR Phase-0.

References

- (1) El-Said, A. S. Nanostructures created in SiO₂ surface: A comparison between the impingement by slow highly charged ions and by swift heavy ions. Nuclear Instruments

- and Methods in Physics Research Section B: Beam Interactions with Materials and Atoms **2012**, 282, 63–67.
- (2) Frost, F.; Ziberi, B.; Schindler, A.; Rauschenbach, B. Surface engineering with ion beams: from self-organized nanostructures to ultra-smooth surfaces. Applied Physics A **2008**, 91, 551–559.
 - (3) Vogel, S.; Linz, S. J. Surface structuring by multiple ion beams. Physical Review B **2007**, 75.
 - (4) Akçöltekin, E.; Peters, T.; Meyer, R.; Duvenbeck, A.; Klusmann, M.; Monnet, I.; Lebius, H.; Schleberger, M. Creation of multiple nanodots by single ions. Nature Nanotechnology **2007**, 2, 290–294.
 - (5) Telkhozhayeva, M.; Girshevitz, O. Roadmap toward Controlled Ion Beam–Induced Defects in 2D Materials. Advanced Functional Materials **2024**, 2404615.
 - (6) Rutherford, E. LXXIX. The scattering of α and β particles by matter and the structure of the atom. The London, Edinburgh, and Dublin Philosophical Magazine and Journal of Science **1911**, 21, 669–688.
 - (7) Bohr, N. I. On the constitution of atoms and molecules. The London, Edinburgh, and Dublin Philosophical Magazine and Journal of Science **1913**, 26, 1–25.
 - (8) Lindhard, J.; Scharff, M.; Schiøtt, H. E. Range Concepts and Heavy Ion Ranges (Notes on Atomic Collisions, II). Matematisk-fysiske Meddelelser, Kongelige Danske Videnskaberne Selskab **1963**, 33, 1–42.
 - (9) Novoselov, K. S.; Jiang, D.; Schedin, F.; Booth, T. J.; Khotkevich, V. V.; Morozov, S. V.; Geim, A. K. Two-dimensional atomic crystals. Proceedings of the National Academy of Sciences of the United States of America **2005**, 102, 10451–10453.

- (10) Lehtinen, O.; Kotakoski, J.; Krasheninnikov, A. V.; Tolvanen, A.; Nordlund, K.; Keinonen, J. Effects of ion bombardment on a two-dimensional target: Atomistic simulations of graphene irradiation. Physical Review B **2010**, 81.
- (11) Krasheninnikov, A. V.; Nordlund, K. Ion and electron irradiation-induced effects in nanostructured materials. Journal of Applied Physics **2010**, 107.
- (12) Schleberger, M.; Kotakoski, J. 2D Material Science: Defect Engineering by Particle Irradiation. Materials **2018**, 11, 1885.
- (13) Liebsch, Y. et al. Quantitative Modeling of Nanopore Formation in 2D MoS₂ by Swift Heavy-Ion Irradiation. ACS Applied Materials & Interfaces **2026**, 18, 7237–7248.
- (14) Kim, J. H.; Jeong, J. H.; Kim, N.; Joshi, R.; Lee, G.-H. Mechanical properties of two-dimensional materials and their applications. Journal of Physics D: Applied Physics **2019**, 52, 083001.
- (15) Cao, Y.; Fatemi, V.; Fang, S.; Watanabe, K.; Taniguchi, T.; Kaxiras, E.; Jarillo-Herrero, P. Unconventional superconductivity in magic-angle graphene superlattices. Nature **2018**, 556, 43–50.
- (16) Cheng, J.; Wang, C.; Zou, X.; Liao, L. Recent Advances in Optoelectronic Devices Based on 2D Materials and Their Heterostructures. Advanced Optical Materials **2019**, 7, 1800441.
- (17) Madauß, L. et al. Highly active single-layer MoS₂ catalysts synthesized by swift heavy ion irradiation. Nanoscale **2018**, 10, 22908–22916.
- (18) Fruehwald, H. M.; Liebsch, Y.; Javed, U.; Lebius, H.; Grygiel, C.; Rahali, R.; Kotakoski, J.; Schleberger, M.; Smith, R. D. L. Basal-Plane Pores Activate Monolayer MoS₂ for the Hydrogen Evolution Reaction. ACS Catalysis **2025**, 15, 3768–3776.

- (19) Junge, F.; Auge, M.; Hofsäss, H. Sputter hot filament hollow cathode ion source and its application to ultra-low energy ion implantation in 2D materials. Nuclear Instruments and Methods in Physics Research Section B: Beam Interactions with Materials and Atoms **2022**, 510, 63–68.
- (20) Lin, P.-C. et al. Doping Graphene with Substitutional Mn. ACS Nano **2021**, 15, 5449–5458.
- (21) Auge, M.; Junge, F.; Hofsäss, H. Laterally controlled ultra-low energy ion implantation using electrostatic masking. Nuclear Instruments and Methods in Physics Research Section B: Beam Interactions with Materials and Atoms **2022**, 512, 96–101.
- (22) Pan, C.-T.; Hinks, J. A.; Ramasse, Q. M.; Greaves, G.; Bangert, U.; Donnelly, S. E.; Haigh, S. J. In-situ observation and atomic resolution imaging of the ion irradiation induced amorphisation of graphene. Scientific Reports **2014**, 4, 6334.
- (23) Ghorbani-Asl, M.; Kretschmer, S.; Spearot, D. E.; Krashennnikov, A. V. Two-dimensional MoS₂ under ion irradiation: from controlled defect production to electronic structure engineering. 2D Materials **2017**, 4, 025078.
- (24) Kozubek, R.; Tripathi, M.; Ghorbani-Asl, M.; Kretschmer, S.; Madauß, L.; Pollmann, E.; O’Brien, M.; McEvoy, N.; Ludacka, U.; Susi, T.; Duesberg, G. S.; Wilhelm, R. A.; Krashennnikov, A. V.; Kotakoski, J.; Schleberger, M. Perforating Free-standing Molybdenum Disulfide Monolayers with Highly Charged Ions. The Journal of Physical Chemistry Letters **2019**, 10, 904–910.
- (25) Akcöltekin, S.; Bukowska, H.; Peters, T.; Osmani, O.; Monnet, I.; Alzaher, I.; d’Etat, B. B.; Lebius, H.; Schleberger, M. Unzipping and folding of graphene by swift heavy ions. Applied Physics Letters **2011**, 98.
- (26) Madauß, L.; Ochedowski, O.; Lebius, H.; Ban-d’Etat, B.; Naylor, C. H.; Johnson, A.

- T. C.; Kotakoski, J.; Schleberger, M. Defect engineering of single- and few-layer MoS₂ by swift heavy ion irradiation. 2D Materials **2017**, 4, 015034.
- (27) Schwestka, J.; Inani, H.; Tripathi, M.; Niggas, A.; McEvoy, N.; Libisch, F.; Aumayr, F.; Kotakoski, J.; Wilhelm, R. A. Atomic-Scale Carving of Nanopores into a van der Waals Heterostructure with Slow Highly Charged Ions. ACS Nano **2020**, 14, 10536–10543.
- (28) Creutzburg, S. et al. Vanishing influence of the band gap on the charge exchange of slow highly charged ions in freestanding single-layer MoS₂. Physical Review B **2020**, 102.
- (29) Hopster, J.; Kozubek, R.; Krämer, J.; Sokolovsky, V.; Schleberger, M. Ultra-thin MoS₂ irradiated with highly charged ions. Nuclear Instruments and Methods in Physics Research Section B: Beam Interactions with Materials and Atoms **2013**, 317, 165–169.
- (30) Zhang, S. X.; Zeng, J.; Hu, P. P.; Xu, L. J.; Maaz, K.; Li, Z. Z.; Liu, L.; Zhai, P. F.; Ai, W. S.; Liu, J. Effects of substrate on swift heavy ion irradiation induced defect engineering in MoSe₂. Materials Chemistry and Physics **2022**, 277, 125624.
- (31) Villarreal, R. et al. Achieving High Substitutional Incorporation in Mn-Doped Graphene. ACS Nano **2024**, 18, 17815–17825.
- (32) Standop, S.; Lehtinen, O.; Herbig, C.; Lewes-Malandrakis, G.; Craes, F.; Kotakoski, J.; Michely, T.; Krasheninnikov, A. V.; Busse, C. Ion impacts on graphene/Ir(111): interface channeling, vacancy funnels, and a nanomesh. Nano Letters **2013**, 13, 1948–1955.
- (33) Ochedowski, O.; Lehtinen, O.; Kaiser, U.; Turchanin, A.; Ban-d’Etat, B.; Lebius, H.; Karlušić, M.; Jakšić, M.; M, S. Nanostructuring graphene by dense electronic excitation. Nanotechnology **2015**, 26, 465302.
- (34) Sleziona, S.; Kharsah, O.; Skopinski, L.; Daniel, L.; Schmeink, J.; Schleberger, M. Influence of Highly Charged Ion Irradiation on the Electrical and Memory Properties

- of Black Phosphorus Field-Effect Transistors. Advanced Electronic Materials **2024**, 2400318.
- (35) Winter, H.; Aumayr, F. Interaction of Slow HCl with Solid Surfaces: What Do We Know, What Should We Know? Physica Scripta **2001**, T92, 15–21.
- (36) Wilhelm, R. A.; Gruber, E.; Schwestka, J.; Kozubek, R.; Madeira, T. I.; Marques, J. P.; Kobus, J.; Krashennikov, A. V.; Schleberger, M.; Aumayr, F. Interatomic Coulombic Decay: The Mechanism for Rapid Deexcitation of Hollow Atoms. Physical review letters **2017**, 119, 103401.
- (37) Wang, Y. Y. et al. Energy deposition by heavy ions: additivity of kinetic and potential energy contributions in hillock formation on CaF₂. Scientific Reports **2014**, 4, 5742.
- (38) Dufour, C.; Khomrenkov, V.; Wang, Y. Y.; Wang, Z. G.; Aumayr, F.; Toulemonde, M. An attempt to apply the inelastic thermal spike model to surface modifications of CaF₂ induced by highly charged ions: comparison to swift heavy ions effects and extension to some others material. Journal of physics. Condensed matter : an Institute of Physics journal **2017**, 29, 095001.
- (39) El-Said, A. S.; Heller, R.; Meissl, W.; Ritter, R.; Facsko, S.; Lemell, C.; Solleder, B.; Gebeshuber, I. C.; Betz, G.; Toulemonde, M.; Möller, W.; Burgdörfer, J.; Aumayr, F. Creation of nanohillocks on CaF₂ surfaces by single slow highly charged ions. Physical review letters **2008**, 100, 237601.
- (40) Hopster, J.; Kozubek, R.; Ban-d'Etat, B.; Guillous, S.; Lebius, H.; Schleberger, M. Damage in graphene due to electronic excitation induced by highly charged ions. 2D Materials **2014**, 1, 011011.
- (41) Skopinski, L.; Kretschmer, S.; Ernst, P.; Herder, M.; Madauß, L.; Breuer, L.; Krashennikov, A. V.; Schleberger, M. Velocity distributions of particles sputtered from sup-

- ported two-dimensional MoS₂ during highly charged ion irradiation. Physical Review B **2023**, 107.
- (42) Niggas, A. et al. Ion-Induced Surface Charge Dynamics in Freestanding Monolayers of Graphene and MoS₂ Probed by the Emission of Electrons. Physical Review Letters **2022**, 129, 086802.
- (43) Grosseck, A. S.; Niggas, A.; Wilhelm, R. A.; Aumayr, F.; Lemell, C. Model for Nanopore Formation in Two-Dimensional Materials by Impact of Highly Charged Ions. Nano Letters **2022**, 22, 9679–9684.
- (44) Bolotin, K. I.; Sikes, K. J.; Jiang, Z.; Klima, M.; Fudenberg, G.; Hone, J.; Kim, P.; Stormer, H. L. Ultrahigh electron mobility in suspended graphene. Solid State Communications **2008**, 146, 351–355.
- (45) Jariwala, D.; Sangwan, V. K.; Late, D. J.; Johns, J. E.; Dravid, V. P.; Marks, T. J.; Lauhon, L. J.; Hersam, M. C. Band-like transport in high mobility unencapsulated single-layer MoS₂ transistors. Applied Physics Letters **2013**, 102.
- (46) Kim, J. H.; Kim, T. H.; Lee, H.; Park, Y. R.; Choi, W.; Lee, C. J. Thickness-dependent electron mobility of single and few-layer MoS₂ thin-film transistors. AIP Advances **2016**, 6.
- (47) Chen, H.; Li, J.; Chen, X.; Zhang, D.; Zhou, P. Dramatic switching behavior in suspended MoS₂ field-effect transistors. Semiconductor Science and Technology **2018**, 33, 024001.
- (48) Yan, J. et al. High-mobility suspended MoS₂ devices with tunable threshold voltage. InfoMat **2026**, e70114.
- (49) Ding, Z.; Jiang, J.-W.; Pei, Q.-X.; Zhang, Y.-W. In-plane and cross-plane thermal conductivities of molybdenum disulfide. Nanotechnology **2015**, 26, 065703.

- (50) Lee, W.-Y.; Kang, M.-S.; Park, N.-W.; Kim, G.-S.; Nguyen, A. D.; Choi, J. W.; Yoon, Y.-G.; Kim, Y. S.; Jang, H. W.; Saitoh, E.; Lee, S.-K. Layer dependence of out-of-plane electrical conductivity and Seebeck coefficient in continuous mono- to multilayer MoS₂ films. Journal of Materials Chemistry A **2021**, 9, 26896–26903.
- (51) Toulemonde, M.; Paumier, E.; Dufour, C. Thermal spike model in the electronic stopping power regime. Radiation Effects and Defects in Solids **1993**, 126, 201–206.
- (52) Ziegler, J. F.; Ziegler, M. D.; Biersack, J. P. SRIM – The stopping and range of ions in matter (2010). Nuclear Instruments and Methods in Physics Research Section B: Beam Interactions with Materials and Atoms **2010**, 268, 1818–1823.
- (53) Yamamura, Y.; Nakagawa, S. T.; Tawara, H. Simulation of low-energy HCI-solid interaction. Nuclear Instruments and Methods in Physics Research Section B: Beam Interactions with Materials and Atoms **1995**, 98, 400–406.
- (54) Insepov, Z.; Allain, J. P.; Hassanein, A.; Terasawa, M. Surface erosion by highly-charged ions. Nuclear Instruments and Methods in Physics Research Section B: Beam Interactions with Materials and Atoms **2006**, 242, 498–502.
- (55) Pálinkás, A.; Kálvin, G.; Vancsó, P.; Kandrai, K.; Szendrő, M.; Németh, G.; Németh, M.; Pekker, Á.; Pap, J. S.; Petrik, P.; Kamarás, K.; Tapasztó, L.; Nemes-Incze, P. The composition and structure of the ubiquitous hydrocarbon contamination on van der Waals materials. Nature Communications **2022**, 13, 6770.
- (56) Ding, Z.; Pei, Q.-X.; Jiang, J.-W.; Huang, W.; Zhang, Y.-W. Interfacial thermal conductance in graphene/MoS₂ heterostructures. Carbon **2016**, 96, 888–896.
- (57) Liao, M.; Wu, Z.-W.; Du, L.; Zhang, T.; Wei, Z.; Zhu, J.; Yu, H.; Tang, J.; Gu, L.; Xing, Y.; Yang, R.; Shi, D.; Yao, Y.; Zhang, G. Twist angle-dependent conductivities across MoS₂/graphene heterojunctions. Nature Communications **2018**, 9, 4068.

- (58) Huo, N.; Wei, Z.; Meng, X.; Kang, J.; Wu, F.; Li, S.-S.; Wei, S.-H.; Li, J. Interlayer coupling and optoelectronic properties of ultrathin two-dimensional heterostructures based on graphene, MoS₂ and WS₂. Journal of Materials Chemistry C **2015**, 3, 5467–5473.
- (59) Desai, S. B.; Madhupathy, S. R.; Amani, M.; Kiriya, D.; Hettick, M.; Tosun, M.; Zhou, Y.; Dubey, M.; Ager, J. W.; Chrzan, D.; Javey, A. Gold-Mediated Exfoliation of Ultralarge Optoelectronically-Perfect Monolayers. Advanced materials (Deerfield Beach, Fla.) **2016**, 28, 4053–4058.
- (60) Pollmann, E.; Sleziona, S.; Foller, T.; Hagemann, U.; Gorynski, C.; Petri, O.; Madauß, L.; Breuer, L.; Schleberger, M. Large-Area, Two-Dimensional MoS₂ Exfoliated on Gold: Direct Experimental Access to the Metal-Semiconductor Interface. ACS Omega **2021**, 6, 15929–15939.
- (61) Bala, A.; Sen, A.; Kim, Y.-H.; Kim, Y.-M.; Gandla, S.; Park, H.; Kim, S. Large-Area MoS₂ Nanosheets with Triangular Nanopore Arrays as Active and Robust Electrocatalysts for Hydrogen Evolution. The Journal of Physical Chemistry C **2022**, 126, 9696–9703.
- (62) El-Said, A. S.; Heller, R.; Aumayr, F.; Facsko, S. Pyramidal pits created by single highly charged ions in BaF₂ single crystals. Physical Review B **2010**, 82.
- (63) Bhowmik, S.; Govind Rajan, A. Size and Chemical Environment Control Nanopore Geometry in 2D MoS₂: From Irregular to Triangular Defects. Small **2025**, 21, e2504611.
- (64) Gong, C.; Colombo, L.; Wallace, R. M.; Cho, K. The unusual mechanism of partial Fermi level pinning at metal-MoS₂ interfaces. Nano Letters **2014**, 14, 1714–1720.
- (65) Peters, T.; Haake, C.; Hopster, J.; Sokolovsky, V.; Wucher, A.; Schleberger, M. HICS: Highly charged ion collisions with surfaces. Nuclear Instruments and Methods in Physics Research Section B: Beam Interactions with Materials and Atoms **2009**, 267, 687–690.

- (66) Skopinski, L.; Ernst, P.; Herder, M.; Kozubek, R.; Madauß, L.; Sleziona, S.; Maas, A.; Königstein, N.; Lebius, H.; Wucher, A.; Schleberger, M. Time-of-flight mass spectrometry of particle emission during irradiation with slow, highly charged ions. The Review of scientific instruments **2021**, 92, 023909.
- (67) Mangler, C.; Meyer, J.; Mittelberger, A.; Mustonen, K.; Susi, T.; Kotakoski, J. A Materials Scientist's CANVAS: A System for Controlled Alteration of Nanomaterials in Vacuum Down to the Atomic Scale. Microscopy and Microanalysis **2022**, 28, 2940–2942.